remote sensing

MDPI

Article

Impact Analysis of Land Use and Land Cover Change on Karez in Turpan Basin of China

Qian Li [1], Huadong Guo [2,3,4], Lei Luo [2,3,4,*], Xinyuan Wang [2,3,4] and Shu Yang [2]

[1] College of Geography and Remote Sensing Sciences, Xinjiang University, Urumqi 830017, China
[2] International Research Center of Big Data for Sustainable Development Goals, Beijing 100094, China
[3] Aerospace Information Research Institute, Chinese Academy of Sciences, Beijing 100094, China
[4] International Centre on Space Technologies for Natural and Cultural Heritage, Beijing 100094, China
* Correspondence: luolei@aircas.ac.cn

Abstract: Karez systems are ancient hydraulic works that use underground waterways to divert water by gravity and have historically been popular in arid regions across Central Asia. Karez systems have undergone thousands of years of development and have been used for irrigation in 40 countries and regions worldwide. Although there are different opinions about the origin of karezes, the role and significance of karezes are similar. The Turpan Basin is a relatively closed inland basin in China, far from the ocean, with a very dry climate and high evaporation rates. However, due to the ice and snow meltwater of the Tianshan Mountains, the groundwater resources in the basin are abundant. Karezes are an important support for Turpan's farming civilization and tourism culture and represent a great masterpiece of how people in arid areas have used the natural environment. This study used historical CORONA images to visually interpret the karez system in the 1970s and compared it with the karez system in 2020 to analyze the spatial distribution variation characteristics of the karezes. The impact of land use/land cover change on the karezes was also analyzed. The results showed that from 1970 to 2020, as the population grew, there was an increase in arable land and built-up areas while the water area decreased. In general, the increase in arable land and built-up areas, the decrease in water area, and the increase in the number of electromechanical wells have combined to reduce the number of karez systems. Based on the CORONA image from 1970, it is possible to visualize the shaft area that existed in 1970 but did not exist in 2020. Some karez shafts that existed in bare terrain areas in 1970 were truncated when the land use/land cover type changed to arable land. The area where the disappeared karez shafts were located is approximately 87.77 square kilometers. Through the study of the changes in the spatial distribution of karezes and the impact of land use/land cover change on karezes, this research provides a valuable reference for the construction of karez conservation areas or urban planning. The investigation of the distribution of historical karezes is of great significance for studying the changes in karezes and excavating the historical and cultural value of karezes.

Keywords: CORONA; active karezes; inactive karezes; LULC

check for updates

Citation: Li, Q.; Guo, H.; Luo, L.; Wang, X.; Yang, S. Impact Analysis of Land Use and Land Cover Change on Karez in Turpan Basin of China. *Remote Sens.* **2023**, *15*, 2146. https://doi.org/10.3390/rs15082146

Academic Editors: Konstantinos X. Soulis and Conghe Song

Received: 9 February 2023
Revised: 5 April 2023
Accepted: 13 April 2023
Published: 19 April 2023

Copyright: © 2023 by the authors. Licensee MDPI, Basel, Switzerland. This article is an open access article distributed under the terms and conditions of the Creative Commons Attribution (CC BY) license (https://creativecommons.org/licenses/by/4.0/).

1. Introduction

Underground irrigation systems in Afghanistan and Central Asia are known as "Kariz". In Xinjiang, China, it is called "karez" in the Uyghur language. In "Shiji" (Records of the Grand Historian of China), it is recorded as "Jingqu" (well and canal). In Persian, it is referred to as "Kanatz-qanat", while in Iran, it is now called "Qanat" [1]. In Pakistan, it is known as "Karezes", while in North Africa, it is referred to as "Foggaras". In the United Arab Emirates, it is known as "Aflaj" [2,3]. As the "karez" system is known as such in the Uyghur language, this study will use "karez" to describe the system.

Karezes are a unique testament to the traditional culture and civilization of the desert in an arid climate. China's karezes were added to the Tentative List of World Cultural Heritage of China in 2008, meeting the Criteria: (I)(IV)(V) [4]. Karez systems are mainly concentrated in the Tuha Basin of Xinjiang, with the Turpan Basin's karez systems having a long history. The number of karez systems in Turpan varies over time, with 1237 channels in 1957. With a history dating back 4000 years, Turpan was once the country of Che Shi 1000 years before the 1st century BC, with the ancient city of Jiaohe as its capital city. From the 1st to the 8th centuries, it was under Han rule, while from the 9th to the 18th centuries, it was the era of the Uighur people. From the Qing Dynasty up to the present, it has been a society of public development for all ethnic groups. Radiocarbon C^{14} dating of eight karez systems in Turpan by Bertil et al. showed that the oldest investigated karez systems originated in the Uyghurian Huihe dynasty (790-1755 AD) [5], indicating that the karez systems in Turpan were created by the local Uyghur people.

Iran has over 30,000 karez systems [1], with 11 Karez systems inscribed on the UNESCO's World Heritage List in 2016. The inclusion criteria were: (iii)(iv) [6]. The Iranian property of the 11 karezes covers an area of 19,057 hectares, and the buffer zone covers an area of 351,343 hectares. Similar to karezes, Aflaj is connected to the natural groundwater level and relies on gravity to pipe groundwater to the villages [7]. The aflaj subterranean tunnel-well system is the most common form of water management in Oman. Historical and archaeological evidence suggests that ancient Greece developed karez-related technology since Classical Times [8].

The landscape of desert cities is fragile, and the karez water conservancy structure represents the ecological wisdom of Iran's Yazd desert city. Environmental planning based on socio-economic methods emphasizing water resources is also an ecological wisdom [9]. Moghadam et al. studied karez water recharge using chemical isotopes and hydrogeological evidence, focusing on six karezes in eastern Iran [10]. Naghedifar et al. [11] developed a numerical simulation model of the karez groundwater system, while Sedghi et al. [12] obtained the solution of the Laplace domain of flow variation of karezes recharged by aquifers under anisotropic unconstraint. Kazemi et al. [13] conducted a health risk assessment study of total chromium in the karezes, which is a historical drinking water supply system. Pueppke [14] reviewed the relationship between water-energy-food in the distant past. The type of land use/land cover is related to the energy exchange of the surface atmosphere and determines the water and carbon exchange between the land and the atmosphere. Accurate land surface conditions are fundamental to environmental and climate research.

Mirani Moghadam et al. [15] analyzed the flow changes of four karezes in eastern Iran over the past 33 years and discussed the factors influencing the changes in karez flow. They showed that since 2000, there has been a significant decrease in precipitation in the study area, while the amount of groundwater pumped through deep wells has increased since 1960 due to the consumption of drinking water and agricultural water, leading to a drop in the groundwater table of 0.1 m per year. The flow rate of the karezes has decreased from 38 L/s to 9 L/s over the past 33 years. At the current rate of groundwater table decline, the four karezes (Rahn, Baidokht, Kheshuie, and Qasabeh) in eastern Iran will disappear in 9–157 years. Therefore, it is necessary to control groundwater extraction and limit water consumption in industry and agriculture [15]. Velasco-Sánchez et al. [16] analyzed changes in soil chemistry in the ancient karez-irrigated agricultural area of southern Jordan. Kowkabi [17] studied ways to restore karezes in Iran to create public open spaces and enhance the quality of social life in urban areas. Delfani et al. [18] studied the thermal effects of karez-source heat pumps. Using the Baladeh karez in eastern Iran as a test area, the impact of suspended solids on water loss during water transport was investigated, and three channels were tested, including the farmland channel, the hand-built channel, and the Baladeh irrigation channel [19]. Barbaix et al. [20] focused on the study of karezes and their location characteristics, using CORONA KH4B, Landsat 8, and Pleiades1 remote sensing imagery to find landscape types of karez, settlements, and vegetation locations. Manian et al. [21] analyzed the risk of COVID-19 transmission in the Kashan karez-irrigated agricultural

area. Keramati et al. [22] compared the concentration of radon 222 in drinking water from spring, well, karez, and tap water, and assessed the health risks of different intakes to adults and children using Monte Carlo simulation (MCS) technology. Ghosh et al. [23] reviewed the risk assessment and treatment measures of coastal aquifer vulnerability to saltwater intrusion and pointed out that Abstraction Desalinization Recharge (ADR) and karez structures can effectively reduce the risk of saltwater intrusion in groundwater extraction areas. However, Sudip et al. [24] reviewed the risks and management techniques associated with saltwater intrusion into coastal aquifers and pointed out that karez structures, shallow, and deep machine wells may be ineffective in reducing seawater intrusion in coastal zone areas because the principle of saltwater intrusion is not fully understood. Samani et al. [25] used five widely used supervised machine learning models to predict the flow rate of karezes with accuracy evaluation indicators, including correlation coefficient, Nash–Sutcliffe efficiency (NSE), RMSE (root means squared error), and MAE (mean absolute error). Karami et al. [26] studied the transient performance of karez source heat pumps using the TRNSYS-MATLAB joint simulator. Sedghi et al. [27] analyzed the semi-analytical solution of flow changes in karezes in alluvial fan aquifers.

Remote sensing archaeology provides a new technological means for archaeology, expanding the temporal and spatial scope of archaeological research. Spatial archaeology is a new paradigm of remote sensing archaeology [28]. Luo et al. [29] summarized the progress of aerospace technology applied to archaeology and cultural heritage over the past century and analyzed the application of ground observation technology in archaeology. Yang et al. [30] used improved Deeplabv3+ and aerial images to automatically extract the Han Great Wall in northwest China, demonstrating the potential of artificial intelligence in remote sensing interpretation. The United Nations' 2030 Agenda for Sustainable Development provides an important guiding framework for economic, social, and environmental development [31]. The Big Earth Data Platform can provide data and methods for assessing various sustainable development indicators. Big data and artificial intelligence technology provide new methods for scientific discovery, and the Big Earth Data Project offers a new paradigm for the study of Earth science [32–34].

The term land use emphasizes the transformation of land types by human society, while land cover refers to the types of land formed by natural environments or human activities [35]. As two-thirds of China's territory is mountainous, changes in land use and land cover are closely related to mountain hazards. Predicting future land use based on historical land use types can provide guidance for the development and utilization of land. Maghrebi et al. [36] used remote sensing techniques to investigate land use/land cover changes in the Mashhad Plain in northern Iran over the past 60 years and the disappearance of 15,983 karezes, showing that only 5.59% of karezes in 1961 were intact in 2021. The most significant land use/land cover changes affecting karezes were agriculture and urban areas, which accounted for 42.93% and 31.81% of karez shaft destruction, respectively. Halik [37] analyzed the impact of spatiotemporal changes in land use/land cover on karez in the Turpan Basin and found that the area of arable land and construction land continued to increase while the water area decreased. This analysis, which used TM/ETM+ images of 1990, 2000, and 2010, directly or indirectly affected the survival of karezes [37]. Yang et al. [38] produced the China land cover dataset (CLCD) with an annual resolution of 30 m using Landsat images and the Google Earth Engine (GEE) platform. They utilized random forests, spatiotemporal filtering, and logical reasoning post-processing methods, achieving an accuracy of 79.31%, which exceeded that of MCD12Q1, ESACCI_LC, FROM_GLC, and GlobeLand30.

Laugier et al. [39] explored the historical land use/land cover of the Upper Diyala/Sirwan River in the Kurdistan Region of Iraq, utilizing satellite remote sensing combined with historical imagery from multispectral sensors of the drone platform and ground geophysical detection. The study revealed that canals, karezes, trackways, and field systems date back to the first millennium CE. Valipour et al. [40] sorted out the sustainable use of groundwater resources from ancient to modern times and even the future, introducing hydrological techniques from Prehistoric Times (3200 BC–1000 BC), Historical Times (1000 BC–330 AD), Medieval Times (ca 330–AD1400), Early and Mid-Modern Times (ca 1400–1900 AD), to Contemporary Times (1900 AD–Present). Climate change or overexploitation may lead to a water crisis. Sayadi et al. [41] conducted a risk assessment of cadmium (Cd) and chromium (Cr) content and growth of edible herbs (Adiantum capillus-verenis, Chara globularis, and Plantago lanceolata) in karez water in 14 villages in the South Khorasan province of Iran from April to August 2018. Assessing the channel stability of karezes under railway pressure is essential as some high-speed railways inevitably pass through the karez area. Zhang et al. [42] used a series of RAFELA (random adaptive finite element limit analysis) methods to investigate the stability of karez channels in cohesive-frictional soils. Ebrahimi et al. [43] reviewed the geoengineering and environmental impacts of the karez system, focusing on determining the location, geometry, depth, and underground passages of karez. Geophysical electrical resistivity tomography (ERT), ground-penetrating radar (GPR), and electromagnetic (EM) methods are commonly used when probing underground pipes and other structural parameters of karezes.

The karez systems in Turpan are a unique form of irrigation that have been used for over 600 years at least. However, in recent years, due to changes in land use and climate, the karez systems have faced serious challenges, such as drying up and collapsing. Therefore, it is of great significance to study the changes in the karez systems and the impact of land use changes on the karez systems. At present, remote sensing technology has become an important means of studying land use changes and the karez systems. The use of high-spatial-resolution remote sensing images to automatically extract the karez systems and study their land use changes can provide important reference data for the rational use and protection of the karez systems. Additionally, understanding the impact of land use changes on the karez systems can provide guidance for the sustainable development of the local economy and agriculture in Turpan. Therefore, the study of the changes in the karez systems and the impact of land use changes on the karez systems is of great significance for the protection and sustainable use of this valuable cultural heritage, as well as for the local economy and agriculture in Turpan.

2. Study Area and Materials

2.1. Study Area

This study focuses on the Turpan Basin, located in the Xinjiang Uyghur Autonomous Region of China. This olive-shaped mountain basin is situated in the eastern part of the Tianshan Mountains. Turpan comprises three administrative units, including Tuoxun County, Gaochang District, and Shanshan County. The administrative scope of Turpan is large and shaped like a parallelogram, with the main area of human activity concentrated in the oasis zone in the north of the administrative region. The oasis is distributed in a narrow band in the east–west direction. Turpan is an essential post station and hub of the Silk Road in the Western Regions, a vital area for cultural exchanges between the East and the West, and a place where the four major civilizations converge. Due to its strategic location, there have been "five fights for Che Shi" in history. Figure 1 shows a map of the study area.

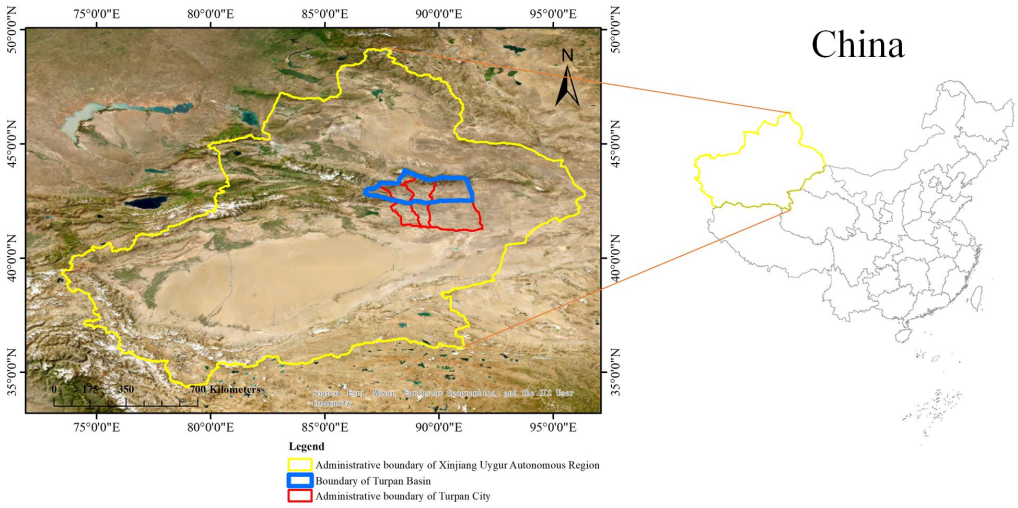


Figure 1. The study area of this paper. The yellow line on the map represents the administrative boundary of the Xinjiang Uyghur Autonomous Region, while the blue line depicts the boundary line of the Turpan Basin. The red line denotes the administrative boundary of Turpan City. The base map used is ArcGIS online imagery World_Imagery. The right side of the figure shows the location of the Xinjiang Uyghur Autonomous Region in China, Asia.

2.2. Karez Data

2.2.1. Karezes of 2000s and 2010s

The data source for karezes in the 2000s was the "Distribution Map of Karez in Xinjiang Uyghur Autonomous Region", compiled by the Xinjiang Second Surveying and Mapping Institute in 2004 [44]. The data source for karezes in the 2010s was the "Integration of the Third National Cultural Relics Census Results in Xinjiang Uyghur Autonomous Region: Karez in Xinjiang", published in 2011 [45]. The data records the number of karezes, as well as their active and inactive status.

2.2.2. Remote Sensing Imagery

The karez data from the 1970s was sourced from historical remote sensing imagery from the CORONA program. The CORONA images are available on the USGS EarthExplorer website (https://earthexplorer.usgs.gov/), accessed on 10 June 2022. The declassified CORONA images from 1966 include KH-1, KH-2, KH-3, KH-4, KH-5, and KH-6. The KH-4, KH-4A, and KH-4B systems carry two panoramic cameras with a separation angle of 30°, with one camera for forward-looking and another for rearview. KH-4A and KH-4B reconnaissance satellites captured each CORONA image, which is typically divided into four small sections during scanning, referred to as "quads". The reason for dividing CORONA images into four quads is for ease of processing and storage. Each quad can be processed separately since its size does not exceed the processor's limit. Additionally, by dividing the image into four quads, it is easier to manage and store large amounts of image data. Each quad's size is usually 6 by 6 inches (about 15 by 15 cm), which means that the length of each quad's side is approximately 8.5 km. These quads are transmitted from the satellite to the ground and then scanned and processed on the ground to generate digital images. The CORONA image used in this study is KH-4B, with a time phase of 19 March 1970. The KH-4B image covering the karez area of Turpan includes five scenes, namely DS1109-2233DF060, DS1109-2233DF061, DS1109-2233DF062, DS1109-2233DF063, and DS1109-2233DF064, with a resolution of 1.8 m. Each scene image is composed of four quads.

The Google Earth imagery is sourced from Google Earth Pro, and the resolution may vary across different regions due to different sensors. For the year 2020, Google Earth has

sub-meter resolution imagery covering the Turpan Basin. The Google imagery is used as a reference to georeference the CORONA imagery in this study.

2.3. Land Use/Land Cover Data

In this study, we analyzed land use changes in Turpan between 1980 and 2020 using land use products with a 10-year interval. Land use/land cover data for the 1980s were obtained from the Landuse dataset in China (1980–2015) [46]. The dataset includes seven periods: the late 1980s, 1990, 1995, 2000, 2005, 2010, and 2015. The dataset was generated by manual visual interpretation of each issue of Landsat TM/ETM+ remote sensing images, with a spatial resolution of 1 km. By merging land use/land cover of different scenes, the Landuse dataset in China (1980–2015) provides a raster format file covering the entirety of China. Using 30-m Landsat multispectral remote sensing imagery to produce 1-kilometer resolution land use/land cover products enables us to obtain higher coverage and a wider spatial range while reducing data processing and storage costs. The one-kilometer resolution land use/land cover products are usually suitable for large-scale land use/land cover studies. The products are projected using the Albers projection method, with a central meridian of 105 and two standard parallels of 1:25 and 2:47. Albers projection is an equal-area conic projection that uses two standard parallels and one standard meridian to define the projection surface, allowing it to maintain the area ratio on the Earth's surface to the maximum extent possible. The types of land use/land cover include 6 primary types and 25 secondary types, with the 6 primary types being arable land, forest land, grassland, water, residential land, and unused land.

The 1992 land cover product used in this study is derived from ESA [47]. The land cover product of ESA CCI is produced based on the 300 m ENVISAT's Medium-Resolution Imaging Spectrometer (MERIS) sensor [48,49]. The format of the land cover product is NetCDF4, and it can be opened in ArcGIS. Subdataset 3 (lccs_class) is the land cover layer. The Land Cover Classification product is the second phase of ESA's Climate Change Initiative (CCI), with a spatial resolution of 300 m. It was offered on an annual scale over a temporal coverage period from 1992 to 2015. The spatial coverage is latitude −90 to 90 degrees, longitude −180 to 180 degrees, and the coordinate system of the data is WGS84 geographic coordinates. The classification criteria for land cover are consistent with the Global Annual Land Cover Classification Series from the 1990s to 2015, produced by the Food and Agriculture Organization of the United Nations Land Cover Classification System (LCCS) and the European Space Agency's (ESA) Climate Change Initiative (CCI) (Figure A1, Appendix A). A total of 22 land types are included. In Land Cover CCI Product User Guide Version 2.0, the 2015 CCI-LC map was validated based on the GlobCover 2009 validation dataset, with a verification accuracy of 71.45% for single- and mixed-ground classes, and 75.4% for single-ground classes. ESA CCI's land use product can be used for studying the response of ecosystem services to land use changes [50]. Gao et al. [35] used ESA land use products to analyze spatiotemporal changes in land use types in the Great Yellow River Basin (the Yellow River Basin, the Huai River Basin, and the Hai River Basin) of China. The study predicted land use scenarios for the year 2030 using the MOLUSCE (Modules for Land Use Change Simulations) plugin in QGIS and analyzed the relationship between land use types and mountain hazards. Tew et al. [51] studied the relationship between land use changes and climate change in the Sungai Kelantan Basin of Malaysia using the ESC CCI land cover data.

The dataset used for Land Use and Land Cover Change (LULCC) analysis between 2000 and 2020 in this study was GlobeLand30 (http://www.globallandcover.com/, accessed on 26 November 2020). GlobeLand30 is the first global geographical information public product provided by China to the United Nations, with the aim of supporting global change research, climate change mitigation, sustainable development implementation, and global governance. The main method used to produce GlobeLand30 is Pixel-object-knowledge-based (POK-based) classification. The product covers the area between 85° south latitude and 85° north latitude with a spatial resolution of 30 m, and producing such

a land use product requires over 10,000 Landsat-like satellite images [52]. GlobeLand30 divides land cover into 10 primary land categories: arable land, woodland, grassland, shrubland, wetlands, water bodies, tundra, artificial surface, bare land, glaciers, and permanent snow cover. The overall accuracy of the GlobeLand30 v2010 data is 83.50%, with a Kappa coefficient of 0.78. The overall accuracy of the GlobeLand30 V2020 data is 85.72%, with a Kappa coefficient of 0.82. The GlobeLand30 data uses the WGS-84 geographic coordinate and UTM projection.

Sun et al. [48] compared six global or national-scale land use and cover datasets (MODIS-MCD12Q1, ESA CCI-LC, GlobeLand30, GLASS-GLC, CAS-CLUDs, and ChinaCover) in the Loess Plateau region of China. The study found that the accuracy of ESA CCI-LC was between 73.9% and 74.2%, which was higher than the accuracy of MODIS and GLASS products. Although GlobeLand30 had an overall accuracy of 86.6% to 86.7%, it could not fully represent the characteristics of returning cropland to forest and grassland in the Loess Plateau. CAS-CLUDs and ChinaCover had the highest accuracy, ranging from 89.4% to 91.6%.

3. Methods

A karez is an ancient underground canal irrigation system mainly distributed in the Turpan area of Xinjiang, China. Its structure consists of a mother well, vertical wells, dragon mouths, open canals, and water tanks, as shown in Figure 2. The vertical wells are typically circular in shape, with a diameter of several meters. The mother well is located at the upstream end of the karez system and is dug beneath the water-bearing layer to divert groundwater into the underground canal. The principle of a karez is to use underground water to enter the mother well and then introduce water into the dragon mouths and open canals through the underground canal, ultimately irrigating farmland or providing water for people's daily life. The functions of the karez's vertical wells include: excavating the soil during the construction of the underground canal, providing ventilation and lighting, determining the direction of the underground canal, providing access for karez craftsmen and maintenance personnel to enter and exit the underground canal, providing tools for the workers in the underground canal, and lifting various equipment. Some vertical wells have well covers to prevent pollution and ensure safety. Open canals are the main channels for directing water to farmland or residential areas, and water can also be stored in water tanks. The advantages of the karez system include water resource conservation, adaptation to arid environments, and minimal energy consumption. A field scene of the karez system is shown in Figure 3.

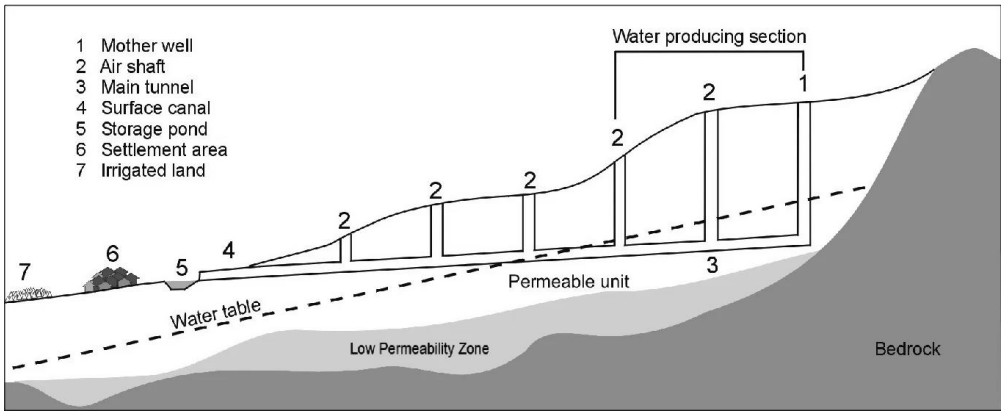


Figure 2. The structural schematic diagram of the karez system is a longitudinal section that shows the various components of the karez system, such as the mother well, vertical wells, dragon mouths, open canals, and water tanks. This diagram is adapted from Abudu's work [53].

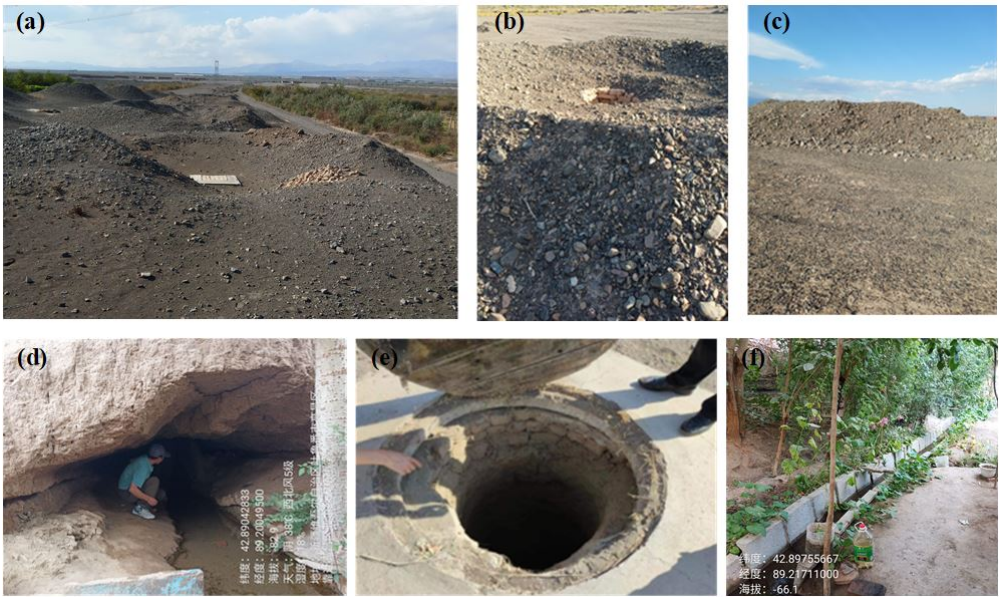


Figure 3. Ground photos of the karez system. Panel (**a**,**b**) show side and top views of the karez shaft. The shaft cover in (**a**) is square, while the shaft in (**b**) has no cover. Panel (**c**) is a side view of the karez shaft, and the wellhead is usually positioned above ground level because during the construction of a karez, a small amount of soil excavated from underground is piled around the wellhead. Panel (**d**) shows the position of the karez dragon mouth. Panel (**e**) is an internal wall view of the karez shaft, with a circular shaft cover. Panel (**f**) shows the open canal of the karez system.

Figure 4 shows that only the vertical wellheads of the karez system are visible on the ground surface and remote sensing images, as the other parts of the karez system are located underground. When mapping the karez system, the vertical wells are abstracted as point features, which is a common practice in geographic information systems (GIS). Discrete features, such as points, lines, and polygons, are used to represent real-world objects in GIS. The location of each vertical well is recorded as a point on the map, enabling the visualization and analysis of the spatial distribution of the karez system. By abstracting the vertical wells as point features, the map can effectively communicate the location and density of the karez system, which is useful for understanding the hydrological and cultural significance of this ancient irrigation system.

The development process of a karez in Turpan can be broadly divided into three stages. The first stage was the slow development stage, which lasted from 1782 to 1845. During this period, the number of karez was limited by the historical population and socio-economic development level, and by the Daoguang period of the Qing Dynasty, the number of karez had grown to close to 300. The second stage was the growth stage, which lasted from 1845 to 1957. After Lin Zexu was demoted to Xinjiang in the 25th year of Daoguang in the Qing Dynasty, he made significant contributions to the development of karezes in Turpan, and by 1912, the early years of the Republic of China, the number of karezes in Turpan had increased to 1060. The third stage was the attenuation stage, which started from 1957 to the present. Since the construction of the first Tianshan system diversion canal in 1957, the water replenishment of karezes has decreased, and the number of karezes has sharply declined from 1237 channels [54]. In the context of climate change, urbanization, and modern technology, the number of mechanical and electrical wells in Turpan has gradually increased, the population has grown, and towns and arable land have expanded. In eastern Xinjiang, temperatures have risen, and precipitation has increased over the past 50–60 years. The Bogda and Miaoergou glaciers have also retreated [55].

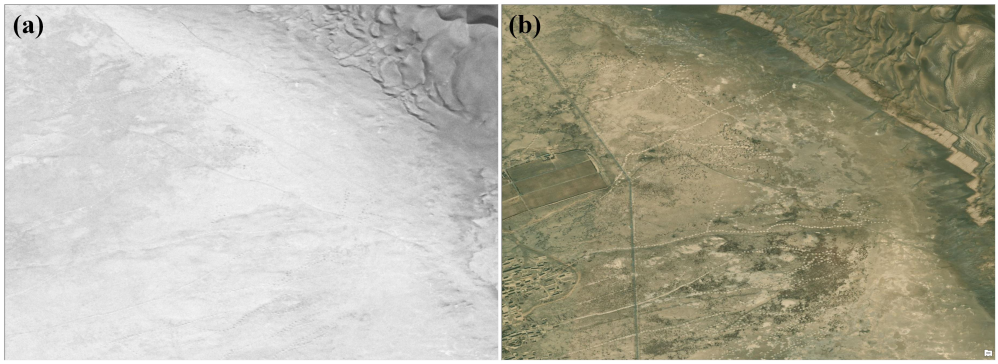


Figure 4. The visual effect of the karez system on remote sensing images is primarily limited to the vertical wellheads, as the other parts of the system are located underground. Figure 4 illustrates this effect, with panel (**a**) showing the karez system on the CORONA panchromatic image and panel (**b**) displaying a map from ESRI's World_Imagery, which is a multi-band image with sub-meter resolution. The vertical wellheads appear as small dots on the images, with their spatial distribution providing insight into the coverage and density of the karez system.

Li et al. [56] utilized the YOLOv5 model and post-processing steps to extract the karez shaft distribution map of the karez system in 2020 using Google Earth imagery. By overlaying the karez map of 2020 with the CORONA image, the karez area can be quickly located using the 2020 karez map as the target area. Although some parts of the karez system may have been abandoned between 1979 and 2020, most of the shafts of the karez system still exist. The karez system is primarily used for the irrigation of farmland and domestic water supply, so the wells are distributed around cultivated land and villages. Therefore, the karez well map in 2020 and spatial distribution characteristics serve as prior knowledge for the visual interpretation of karez wells on the CORONA imagery. Using CORONA images as the data source, this study analyzes the distribution of karezes in the 1970s through visual interpretation and compares it with the distribution of karezes in 2020 to analyze changes in the karez system. The study also obtains the land use/land cover transfer matrix of the Turpan Basin in the past 40 years by analyzing the land use/land cover changes in the region and explores the impact of land use/land cover change on the karez system. When comparing different maps, the projection method should be consistent. Based on the longitude range of Turpan, the study area of this article, the projection is UTM projection with zone number 45N, and the geodetic datum is WGS84. The technical route flowchart of this study is presented in Figure 5.

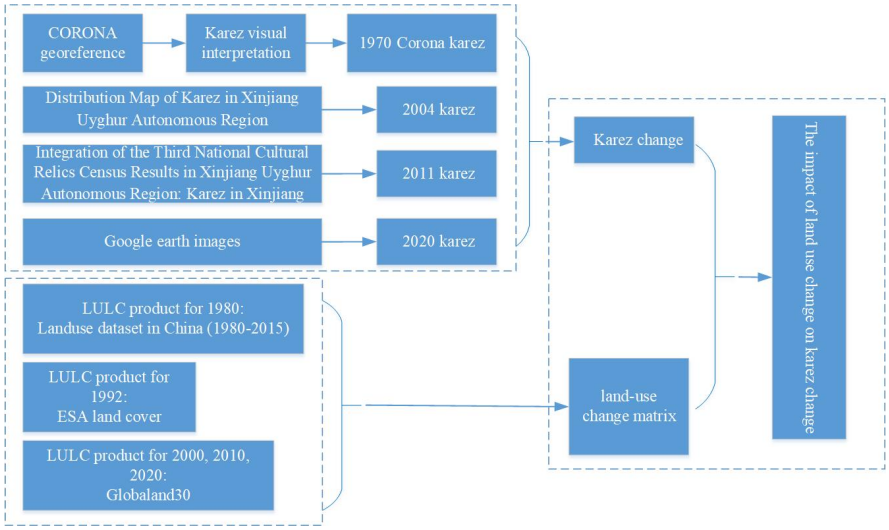


Figure 5. The overall technical roadmap for the analysis of the impact of land use/land cover change on karez in the Turpan Basin.

3.1. CORONA Images Processing

The CORONA images downloaded from USGS are not strictly georeferenced, as they only provide the four-solstices coordinates of the image, which are not particularly accurate. In order to ensure that remote sensing images of different time phases can be superimposed and analyzed, geometric correction is necessary. The preprocessing of the CORONA images includes intra-scene stitching and georeferencing. In single-scene stitching, the pixel difference of overlapping left and right, upper and lower edges is calculated using ENVI, and then splicing is carried out based on the PIL module of the Python program. Georeferencing is based on very high-resolution Google Earth imagery. The ArcGIS georeferencing tool is used for correction, and the correction method adopts the spline model, which requires the number of GCPs (Ground Control Points) to be greater than 10. The control point error is 0, and the number of control points for each image is shown in Table 1. Spline functions are piecewise polynomial functions that guarantee continuity and smoothness between adjacent polynomials. Spline functions accurately transform source control points to target control points. The higher the number of control points, the higher the overall accuracy of the spline transformation. The number of karez systems included in different imagery varies, and only the target area of this study, i.e., the region where karez systems exist, is accurately spine-corrected when performing geometric correction on CORONA imagery. Therefore, the number of control points used for correction varies significantly between different images. The resampling method uses Nearest Neighbor.

Table 1. The number of control points for georeferencing the CORONA images.

The Image id	Number of Control Points (pcs)
DS1109-2233DF060_b.tif	14
DS1109-2233DF060_d.tif	16
DS1109-2233DF061.tif	113
DS1109-2233DF062.tif	94
DS1109-2233DF063.tif	28
DS1109-2233DF064.tif	13

3.2. Karez Change

This study conducted a statistical analysis of the number of active and inactive karez systems at the township administrative level for the 2000s and 2010s. The linear feature was used as the statistical unit, with each karez system counted as one unit, and the change in the number of karez systems between these two time periods was analyzed. Visual interpretation was used to analyze the changes in the vertical shafts of karez systems between CORONA imagery and the shafts in 2020 extracted by Li et al. [56]. Additionally, we calculated the area of the region where the vertical wells of karez systems changed between 1970 and 2020.

3.3. Land Cover Change

To unify the land use types for the analysis of land use change, the land use types in the Landuse dataset in China (1980–2015) and ESA were matched to the primary land use categories of Globaland30. This was necessary because the land use types in these datasets were not completely consistent. Merging similar land use types into a general primary category can reduce the complexity of classification. The 25 secondary land use categories in the Landuse dataset in China (1980–2015) were merged into 10 primary categories consistent with Globaland30, as shown in Table 2. For example, high-coverage grass, medium-cover meadow, and low-cover grass were merged into the grassland category, while forest land, shrubland, sparse forest land, and other forest land were merged into the forest land category. The categories of land use products from three sources were aligned by merging categories, using rules similar to the specifications for studying the response of ecosystem services to land use changes [50].

Table 2. Reclassification of 25 land classes in the Landuse dataset in China (1980–2015) into 10 land categories consistent with Globaland30.

Primary Classification	Secondary Classification	Reclassified
cultivated land	-	
-	paddy field	Cropland
-	dry land	Cropland
woodland	-	
-	Forest land	Forest
-	Shrubland	Shrubland
-	Sparse forest land	Forest
-	Other forest land	Forest
grassland	-	
-	High coverage grass	Grassland
-	Medium cover meadow	Grassland
-	Low cover grass	Grassland
waters	-	
-	Canals	Water
-	lakes	Water
-	Reservoir pits	Water
-	Permanent glacial snow	Permanent snow and ice
-	Beach	Water
-	Beach	Water
Urban and rural, industrial and mining, residential land	-	
-	Town land	Settlement
-	Rural settlements	Settlement
-	Other construction land	Settlement
Unused land	-	
-	Sandy land	Bare land
-	Gobi	Bare land
-	Saline land	Bare land
-	marshland	Wetland
-	Bare land	Bare land
-	Bare rock texture	Bare land
-	other	Bare land

The 22 land use types in ESA were also merged into 10 land use categories consistent with Globaland30. For example, consolidated bare areas and unconsolidated bare areas were merged into the bare land category, and shrubland, evergreen shrubland, and deciduous shrubland were merged into the shrubland category. In a study of ecosystem services on Madagascar Island, Africa, ESA CCI land cover types were merged into eight categories [50], which differs from this study, where the land categories include permanent snow and ice and lichens and mosses. Although the Turpan region has distributions of permanent snow and ice land types, it does not have lichens and mosses land types. The rules for reclassification are shown in Table 3.

The reclassification of land cover was carried out using ArcGIS software. The Join and Relates tool was used to associate an Excel file containing the correspondence between secondary classifications and reclassified classifications based on the code field with a raster map of land use/land cover types. This allowed each pixel of the raster data to be assigned the attributes of a primary land class. The Raster to Polygon tool in ArcGIS 10.2 was then used to convert the land use types of the raster structure into a vector format. The Dissolve tool was used to merge different objects of the same reclassified land use category based on the Dissolve_Field(s) (optional) option. The attribute table of the vector layer generated by Dissolve provided the total area of the various land classes in the reclassified ground class.

To obtain the land type transition map for different years, the Intersect tool was used to intersect vector layers of different years. The area field was added to the attribute table of the land use/land cover distribution vector map obtained by Intersect, and the area was calculated using the field calculator. The attribute table was then converted to Excel format, and a land use/land cover transfer matrix was created using the Excel pivot table function.

Table 3. Mapping table for reclassifying ESA landcover's 22 land classes into 10 reclassified land classes consistent with Globaland30.

Code	Reclassified	ESA-LC/CCI-LC
10	Cropland	Cropland, rainfed
11	Cropland	Herbaceous cover
12	Cropland	Tree or shrub cover
20	Cropland	Cropland, irrigated or post-flooding
30	Cropland	Mosaic cropland (>50%)/natural vegetation (tree, shrub, herbaceous cover) (<50%)
40	Cropland	Mosaic natural vegeation (tree, shrub, herbaceous cover) (>50%)/cropland (<50%)
50	Forest	Tree cover, broadleaved, evergreen, closed to open (>15%)
60	Forest	Tree cover, broadleaved, deciduous, closed to open (>15%)
61	Forest	Tree cover, broadleaved, deciduous, closed (>40%)
62	Forest	Tree cover, broadleaved, deciduous, open (15–40%)
70	Forest	Tree cover, needleleaved, evergreen, closed to open (>15%)
71	Forest	Tree cover, needleleaved, evergreen, closed (>40%)
72	Forest	Tree cover, needleleaved, evergreen, open (15–40%)
80	Forest	Tree cover, needleleaved, deciduous, closed to open (>15%)
81	Forest	Tree cover, needleleaved, deciduous, closed (>40%)
82	Forest	Tree cover, needleleaved, deciduous, open (15–40%)
90	Forest	Tree cover, mixed leaf type (broadleaved and needleleaved)
100	Forest	Mosaic tree and shrub (>50%)/herbaceous cover (<50%)
110	Grassland	Mosaic herbaceous cover (>50%)/tree and shrub (<50%)
120	Shrubland	Shrubland
121	Shrubland	Evergreen shrubland
122	Shrubland	Deciduous shrubland
130	Grassland	Grassland
140	Lichens and mosses	Lichens and mosses
150	Forest	Sparse vegetation (tree, shrub, herbaceous cover) (<15%)
152	Shrubland	Sparse shrub (<15%)
153	Grassland	Sparse herbaceous cover (<15%)
160	Forest	Tree cover, flooded, fresh or brakish water
170	Forest	Tree cover, flooded, saline water
180	Wetland	Shrub or herbaceous cover, flooded, fresh/saline/brakish water
190	Settlement	Urban areas
200	Bare land	Bare areas
201	Bare land	Consolidated bare areas
202	Bare land	Unconsolidated bare areas
210	Water	Water bodies
220	Permanent snow and ice	Permanent snow and ice

4. Results

4.1. Karez Change

The Xinjiang Second Institute of Surveying and Mapping compiled a "Distribution Map of Karez in Xinjiang Uyghur Autonomous Region" in 2004, which revealed that there were a total of 926 karezes in the 31 townships of the Turpan Basin. Among them, 322 karezes were active, 430 were inactive, and 174 were recoverable. Figure 6 shows the number of active, inactive, and recoverable karezes in each township. In some townships, the number of inactive karezes exceeded 100. The three townships with a total number of karezes over 100 were Katsukin Township, Yar Township, and Dican Township. Yar Township had the highest number of active karezes in 2004, with 66 karezes. This township is located in the western suburbs of Turpan City and belongs to Gaochang District in the Xinjiang Uyghur Autonomous Region.

The "Collection of Results of the Third National Census of Cultural Relics in Xinjiang Uyghur Autonomous Region" published in 2011, reported a total of 1108 karezes in the 31 townships of the Turpan Basin. Among them, 278 karezes were active, and 830 were inactive. Figure 7 shows the number distribution of active and inactive karezes in each township. It is evident from the figure that the number of inactive karezes in most townships is much larger than the number of active karezes. There are four townships with a total number of karezes of over 100, namely Chatkale Township, Katsukin Township, Yar Township, and Dican Township. Yar Township had the highest number of active karezes in 2011, with 49 karezes.

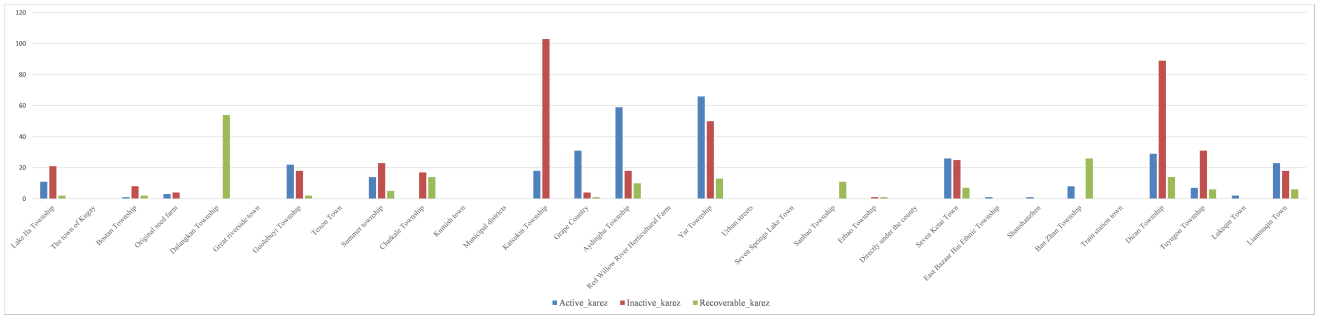


Figure 6. Comparison of the number of active karezes, inactive karezes, and recoverable karezes in the 31 townships of the Turpan Basin in 2004.

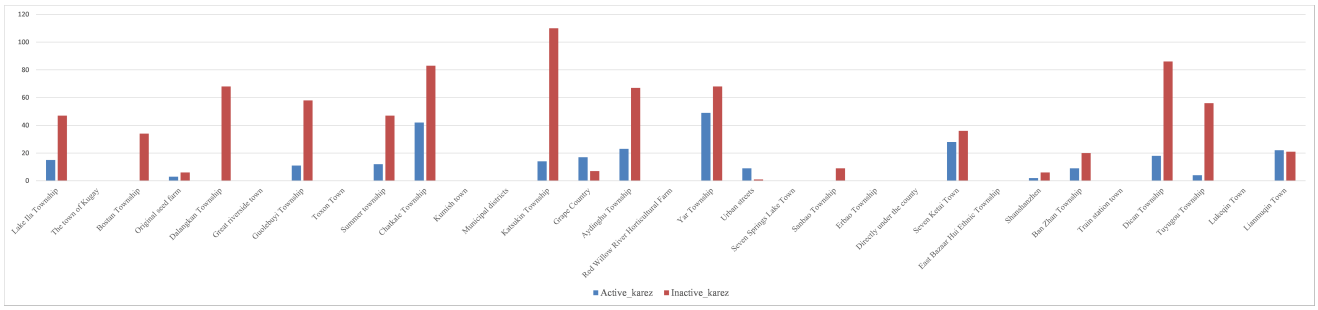


Figure 7. Comparison of the number of active karezes and inactive karezes in 31 townships in the Turpan Basin in 2011.

4.2. LULC Change

Figure 8 shows the distribution of land use/land cover types in the Turpan Basin at 10-year intervals from 1980 to 2020. The Turpan region is located in an arid area and has 9 out of the 10 reclassified land types, excluding moss-free and lichen-free. Forest was present in 1992 but not in 2000 or 2010. However, forests were present again in 2020. The land classification map indicates that the three main land surface types in Turpan are bare land, grassland, and cultivated land.

Table 4 shows the total land use/land cover transfer matrix from 1980 to 2020 in the Turpan Basin. Moreover, Tables A1–A4 in Appendix A show the land use/land cover transfer matrix for each adjacent 10 years from 1980 to 2020 in the Turpan Basin. Using these data, a Sankey visualization map was created and is presented in Figure 9.

The Turpan Basin is dominated by bare land, followed by grassland, with forest and farmland having much smaller areas than the former two. To better visualize the differences in the area between different land types, we compare the four land types of bare land, grassland, farmland, and forest, and the five land types of the urban area, shrub, water, wetland, glacier, and permanent snow. Figure 10 shows a histogram comparing the area of the nine land classes and multi-temporal ground classes divided into two groups.

Table 4. The land use/land cover area transfer matrix from 1980 to 2020 in the Turpan Basin.

Reclassified Class (km^2)	Bare Land	Cropland	Forest	Grassland	Permanent Snow and Ice	Settlement	Shrubland	Water	Wetland	Sum
Bare land	19139	271	0	3090	55	180	4	5	2	22,746
Cropland	42	733	0	165	0	98	3	1	0	1044
Forest	34	68	7	112	0	8	0	0	0	230
Grassland	3419	356	19	8657	22	60	11	2	1	12,549
Permanent snow and ice	120	0	0	131	20	0	0	0	0	272
Settlement	37	35	0	14	0	27	0	0	0	113
Shrubland	8	2	0	3	0	0	1	0	0	14
Water	5	1	0	10	0	0	0	0	0	17
Sum	22,805	1467	27	12,183	97	374	20	9	3	36,985

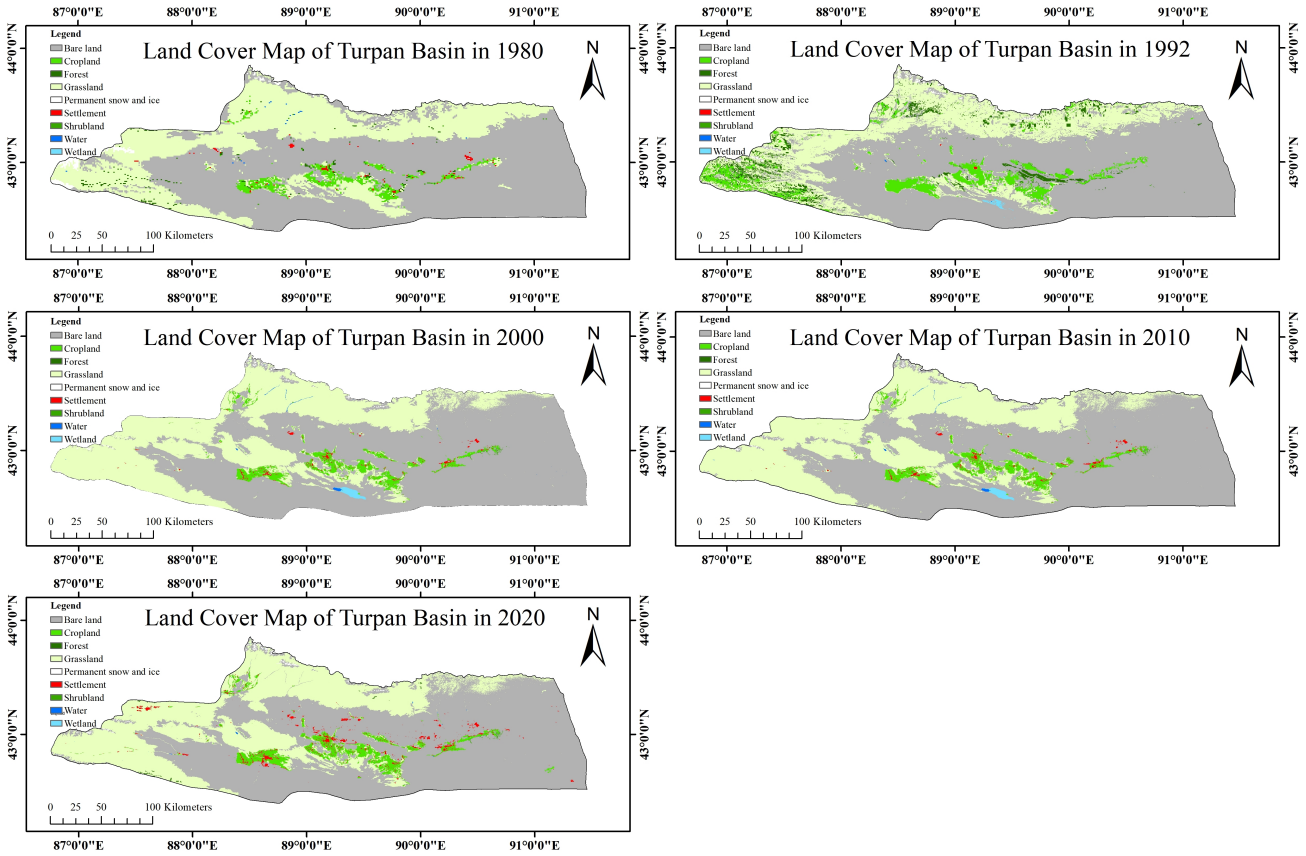


Figure 8. Land use/land cover distribution of the Turpan Basin at 10-year intervals from 1980 to 2020.

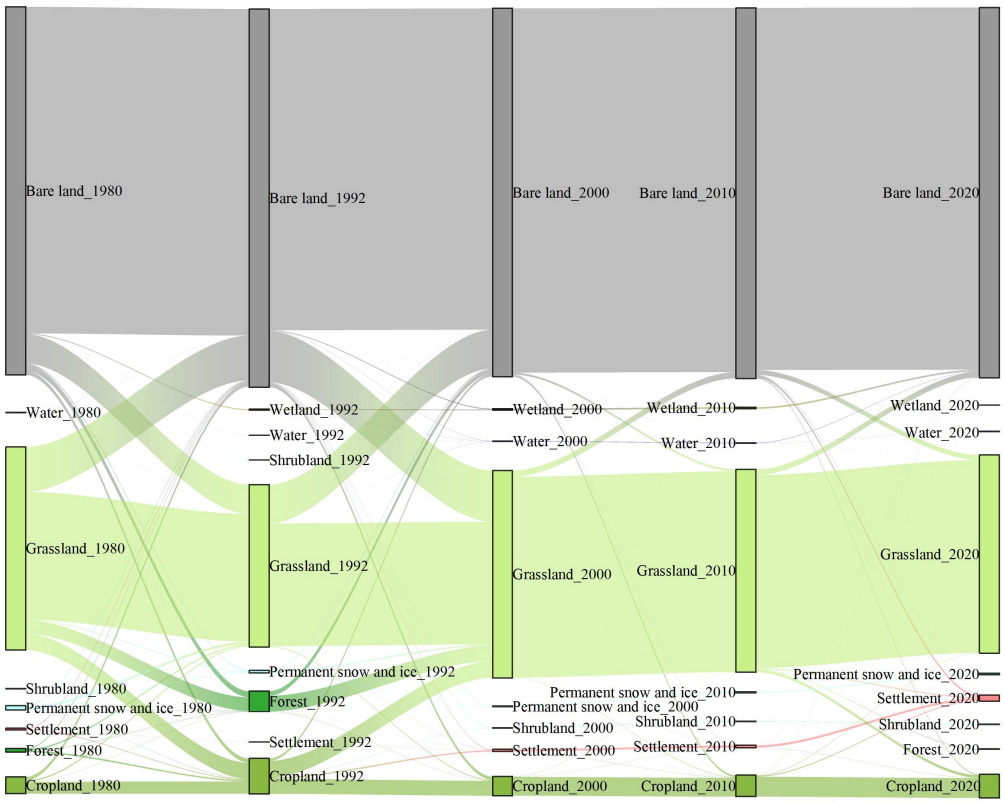


Figure 9. A Sankey diagram representing the transformation of reclassified land classes in the Turpan Basin from 1980 to 2020.

To better illustrate the changes in land use/land cover types in the Turpan Basin, a three-dimensional map is presented in Figure 11, which shows the changes in various land use/land cover types in the Turpan Basin from 1980 to 2020.

By analyzing Figures 10 and 11, the overall trend from 1980 to 2020 in the Turpan Basin can be summarized as follows:

- The built-up area has significantly increased over time.
- The area of cultivated land has increased consistently.
- The area of shrubland has also increased.
- The area of forest has decreased significantly over time.
- The area of permanent snow and glaciers has decreased.
- The area of water and wetlands shows a trend of first increasing and then decreasing.
- The areas of bare land and grassland remain relatively stable.

During the period of 1980–2020, the area of cultivated land consistently increased, except for 1992, when it was significantly higher than in other years. The built-up area also showed a stable growth trend in other years, except for 1992, when its area was lower than in other years.

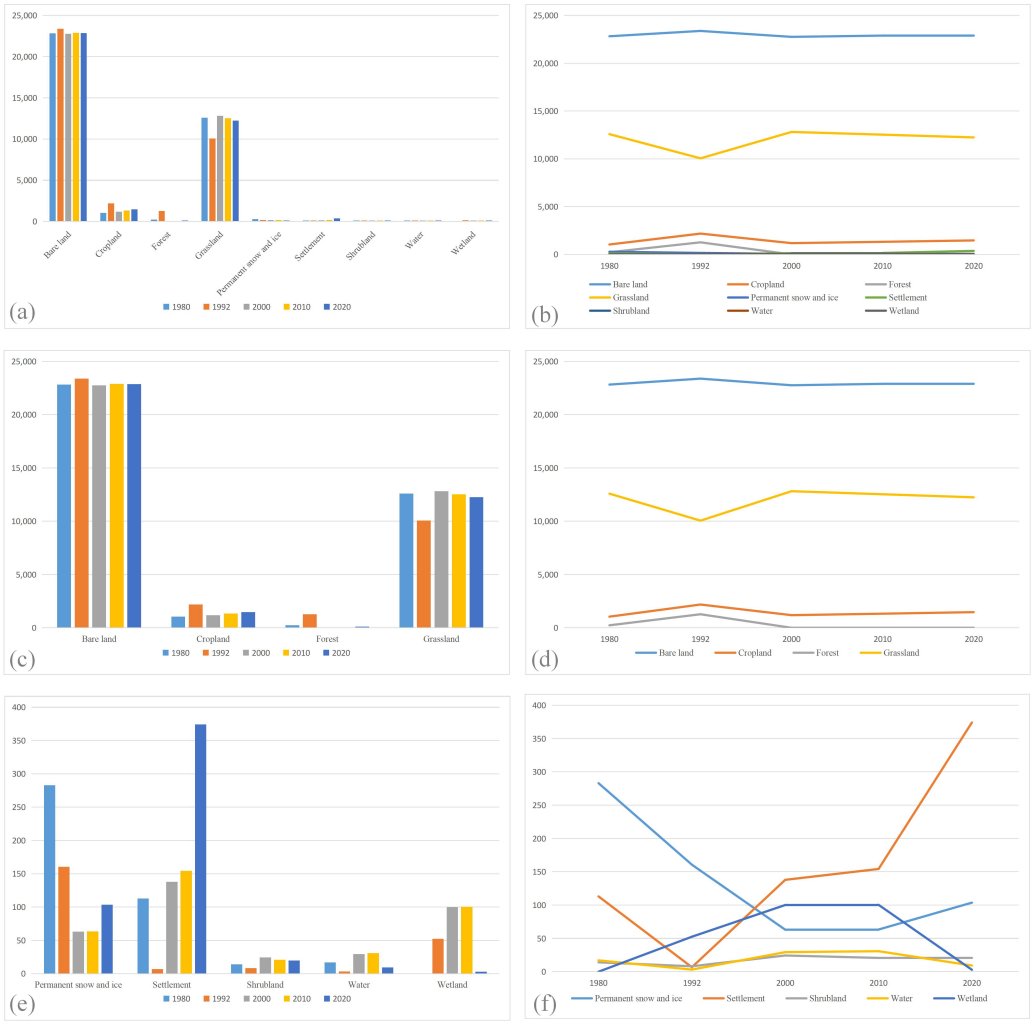


Figure 10. Three sets of graphs. The first set shows a statistical histogram (**a**) and a line chart (**b**) of the area of the nine reclassified land types in the Turpan Basin from 1980 to 2020. The second set shows a statistical histogram (**c**) and a line chart (**d**) of the area of the four reclassified land types in the Turpan Basin, including bare land, grassland, arable land, and forest land, from 1980 to 2020. The third set shows a statistical histogram (**e**) and a line chart (**f**) of the area of the five reclassified land types in the Turpan Basin, including permanent snow and glaciers, residential areas, shrubs, waters, and wetlands, from 1980 to 2020.

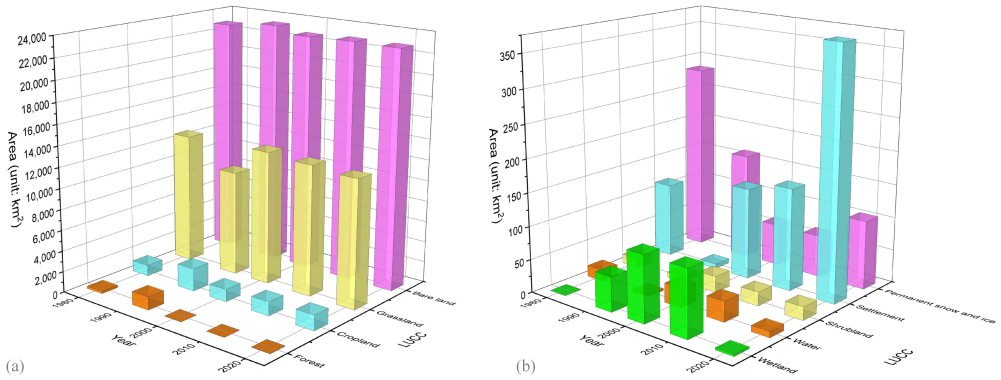


Figure 11. Two histograms. The first histogram (**a**) shows the area of four reclassified land types in the Turpan Basin, including bare land, grassland, arable land, and forest land, from 1980 to 2020. The second histogram (**b**) shows the area of five reclassified land types, including permanent snow and ice, residential areas, shrubs, waters, and wetlands, in the Turpan Basin from 1980 to 2020.

According to previous research [57], the population of Turpan has steadily increased from 1985 to 2020, as shown in Figure 12. Therefore, it is reasonable to expect that the areas of cultivated land and built-up land would also steadily increase during this period. This trend is consistent with the observed changes in land use/land cover types in the Turpan Basin.

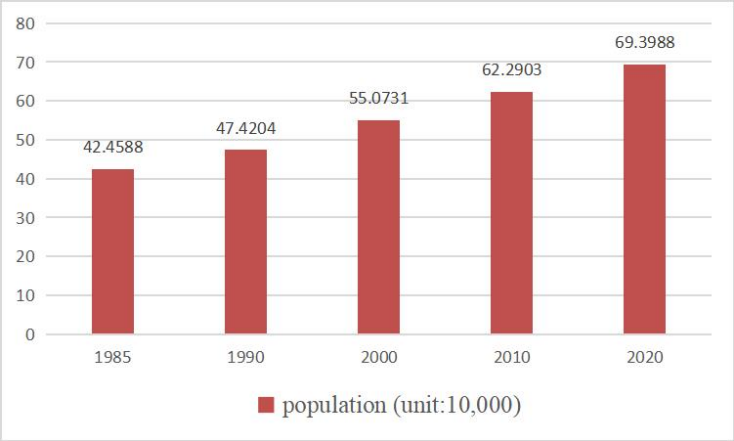


Figure 12. Population trend in Turpan City from 1985 to 2020.

4.3. Influence of LULC Change on Karez Change

This study analyzed the impact of land use/land cover changes on the karez system in the Turpan Basin by comparing the distribution of karezes in 1970 on a CORONA image with karezes in 2020 [56]. As shown in Figures 13 and 14, some karezes located on bare land were truncated when the land use/land cover changed to arable land. The disappeared karez shafts cover an area of approximately 87.77 square kilometers. The population of the Turpan Basin has gradually increased, and the area of urbanization has expanded over time. With the increase in water demand and the advent of electromechanical well technology [37], the use and maintenance of the karez system have gradually decreased, leading to its decline.

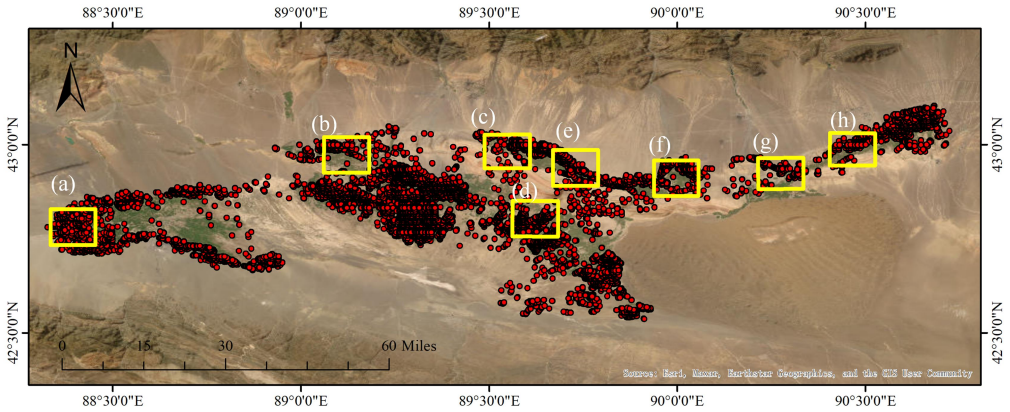


Figure 13. A karez map of the Turpan Basin, with a red dot representing the location of a karez shaft in 2020. The map also features eight yellow rectangular boxes (a)–(h). The local magnified views of (a)–(h) are shown in Figure 14. The base map used is the ArcGIS online imagery World_Imagery.

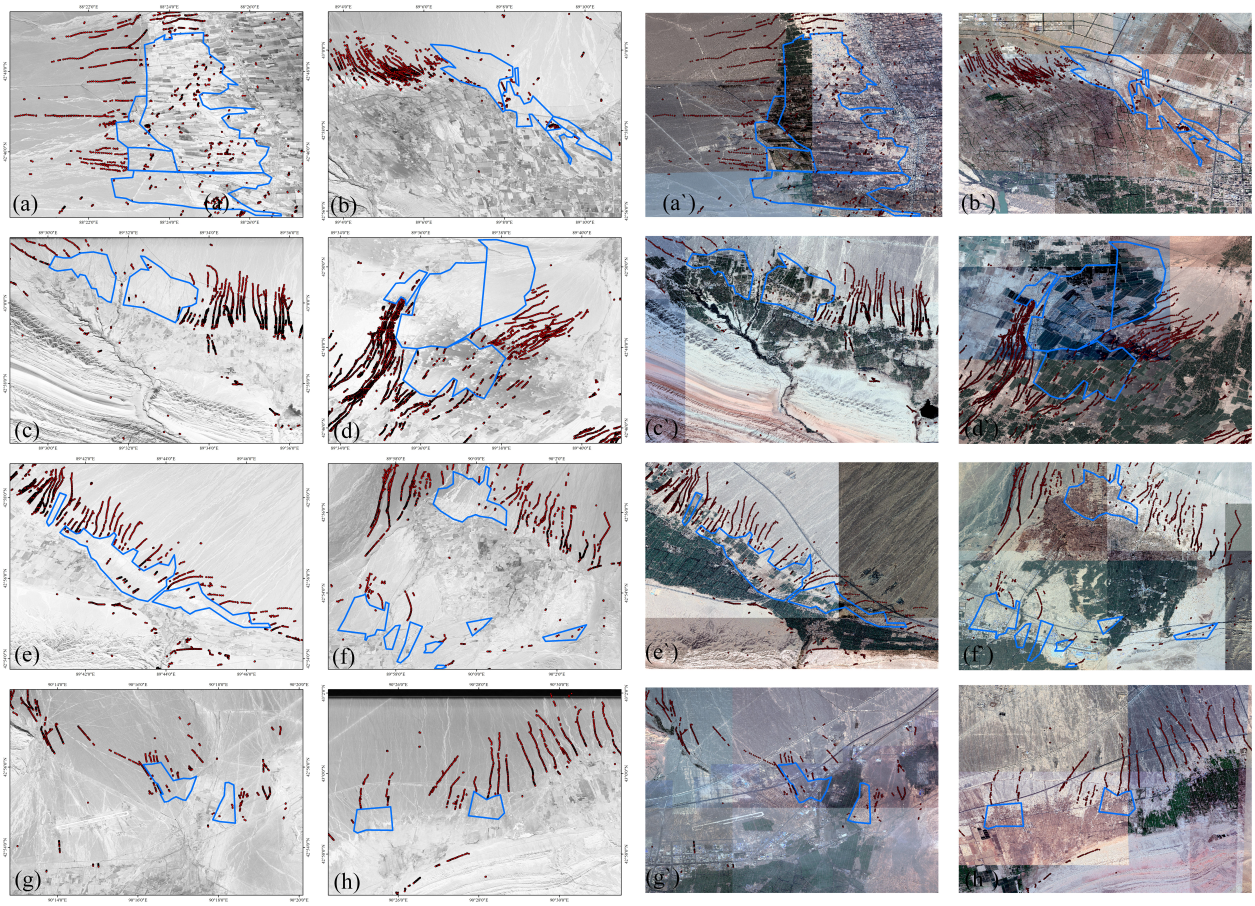


Figure 14. The red dots show the karez shafts in 2020, and the blue polygon shows the area where the karez shafts existed in 1970 but did not exist in 2020. (**a**–**h**,**a′**–**h′**) correspond to the eight yellow boxes in Figure 13, respectively. The base maps for (**a**–**h**) are CORONA imagery, while the base maps for (**a′**–**h′**) are Google imagery from 2020.

The vector map of the area where the shafts were present in 1970 but disappeared in 2020 was overlaid with the land use types in 2020, and the Zonal Histogram tool in ArcGIS 10.2 was used to count the corresponding land use types in the vector map for 2020. The results are shown in Figure 15. According to the statistical results, the land use types in

the area where the karez shafts existed in 1970 were mainly cropland, bare land, grassland, and built-up areas in 2020. Among them, cropland had the largest proportion, accounting for 67.81%, while bare land and grassland accounted for 12.3% and 11.26%, respectively. The proportion of built-up areas was 8.61%. This indicates that the main change in land use types leading to the disappearance of the shafts was the conversion of bareland to cropland. The expansion of built-up areas also occupied some of the land previously used for shafts.

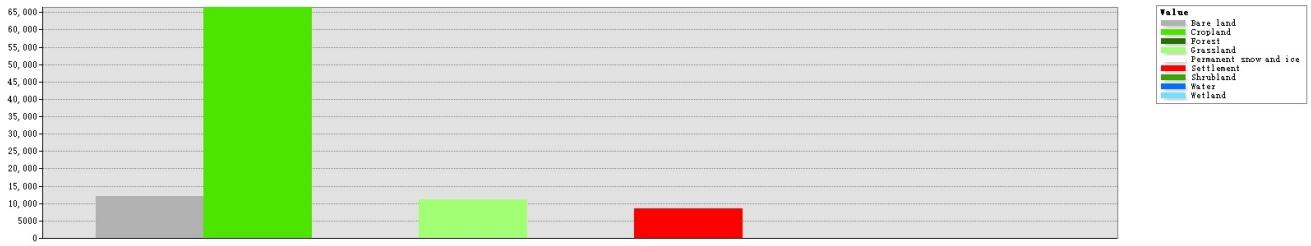


Figure 15. Histograms of LULC in 2020 in zones of the area where the shafts existed in 1970 and disappeared in 2020. The vertical axis is in pixels.

5. Discussion

The Turpan karez system is a traditional underground irrigation system in the Xinjiang region, which has been an important support for agricultural production in the area since ancient times. However, with the influence of climate change and human activities in recent years, the number and status of Turpan karezes have undergone significant changes, which have also affected local agricultural production. Based on historical remote sensing imagery data from CORONA and field investigations, it has been found that the number of Turpan karezes has significantly decreased over the past few decades. Some karezes have lost their irrigation function due to a long-term lack of maintenance and management and have become abandoned, while others are in varying degrees of damage and decay. These changes are mainly due to the influence of human activities, such as excessive groundwater exploitation, land use change, and urbanization, as well as the impact of climate change, such as increased extreme weather events.

The changes in Turpan karezes have had a significant impact on agricultural production in the region. Due to the lack of sufficient irrigation water sources, agricultural production has been severely limited, leading to problems such as decreased crop yield and land degradation. In addition, the decline of karezes has also brought adverse effects on local social and economic development, such as labor force loss and income reduction. Therefore, in order to protect the Turpan karezes and promote sustainable development in the region, a series of measures need to be taken, including strengthening the management and protection of groundwater resources, promoting water-saving irrigation technology, and improving land use planning and urbanization management.

The Turpan Karez Park offers a comprehensive display of the structure, culture, and history of the karez system, providing not only a place for the inheritance of karez culture but also cultural enrichment for tourism development. Karez systems are a testament to the wisdom of people living in arid areas to adapt to their environment and have served as the lifeline of oasis civilizations throughout history. Karez systems represent a sustainable way of using water resources and can serve as a reference for the construction of ecological civilization.

6. Conclusions

Turpan Karez Park presents a relatively complete display of the structure, culture, and history of karezes. It serves as a site for the preservation of karez culture and provides cultural significance for the development of tourism. Karez systems are the crystallization of the wisdom of the people of arid areas to adapt to the environment,and are the lifeline of oasis civilization in history. Karez systems are a sustainable way to use water resources and can provide a reference for the construction of ecological civilization. Studying the impact

of land use/land cover change on karezes can provide a reference for karez protection and maintenance. The extraction of spatial distribution information of karezes can also provide a basis for the delineation of core areas and buffer zones for karez protection.

Remote sensing technology has the advantages of providing macroscopic, objective, and dynamic monitoring of the Earth's surface. This study used historical CORONA images to visually interpret the karez system in the 1970s. By analyzing land use/land cover changes at different times, a land use/land cover transfer matrix and land transfer visualization were obtained. The results showed that from 1970 to 2020, as the population grew, the demand for arable land and built-up areas increased, resulting in an increase in arable land and built-up areas, while the water area decreased. With the advent of electromechanical well technology and the increase in the number of such wells, the maintenance and utilization of karezes have gradually decreased. In general, the increase in arable land and built-up areas, the decrease in water area, and the increase in the number of electromechanical wells have combined to reduce the number of karez systems. By comparing the CORONA image from 1970 with the karez shafts in 2020, it is possible to visualize the karezes that existed in 1970 but did not exist in 2020. Some karez shafts that existed on bare terrain areas in 1970 were truncated when the land use/land cover changed to arable land.

Overall, the Turpan karez system is a valuable cultural and ecological resource, and its protection and sustainable use are of great significance. The use of remote sensing technology and historical data has provided valuable insights into the changes in the Karez system and the impact of land use/land cover changes on the system in the Turpan Basin. These findings can provide valuable information for karez protection and maintenance. The spatial distribution information of karezes can also provide a basis for the delineation of core areas and buffer zones for karez protection, promoting sustainable development in the region.

Author Contributions: Conceptualization, Q.L., H.G. and X.W.; methodology, Q.L., X.W., L.L. and S.Y.; software, Q.L.; validation, Q.L. and X.W.; formal analysis, Q.L. and L.L.; investigation, L.L.; resources, H.G. and L.L.; data curation, Q.L., X.W. and L.L.; writing—original draft preparation, Q.L.; writing—review and editing, X.W. and L.L.; visualization, Q.L.; supervision, L.L.; project administration, H.G.; funding acquisition, H.G. All authors have read and agreed to the published version of the manuscript.

Funding: This work was funded by the Construction of the China-Central Asia Human and Environment "Belt and Road" Joint Laboratory and Joint Research on Ancient Human Culture and Environment in the Sulh River Basin (Grant No. 2022YFE0203800, November 2022 to October 2025), the Youth Innovation Promotion Association of CAS (Grant No. 2023135), and the Innovative Research Program of the International Research Center of Big Data for Sustainable Development Goals (Grant No. CBAS2022IRP09).

Data Availability Statement: The corresponding author will provide the data upon request.

Acknowledgments: The authors would like to thank Long Wang, who is of the Institute of Archaeology of the Turpan Research Institute, and Gang Li, Deputy Research Librarian of the Turpan Research Institute, for providing the information of the karez, and Mulati Najimuding of the Cultural Relics Protection Department of the Gaochang District Bureau of Culture, Sports and Tourism of Turpan City for leading the author to conduct field research on the karez. Thanks to Yang Shu for his assistance in sorting out the information of karezes.

Conflicts of Interest: The authors declare no conflict of interest.

Appendix A

Table A1. Land use/land cover area transfer matrix from the year 1980 to 1992 in the Turpan Basin.

Reclassified Class (km^2)	Bare Land	Cropland	Forest	Grassland	Permanent Snow and Ice	Settlement	Shrubland	Water	Wetland	Sum
Bare land	20,167	260	374	1803	79	0	6	3	52	22,744
Cropland	210	747	10	75	0	1	0	0	0	1044
Forest	48	86	16	81	0	0	0	0	0	230
Grassland	2774	1003	841	7890	39	0	2	0	0	12,549
Permanent snow and ice	62	25	20	130	35	0	0	0	0	272
Settlement	48	45	2	12	0	6	0	0	0	113
Shrubland	6	5	1	3	0	0	0	0	0	14
Water	5	1	2	9	0	0	0	0	0	17
Sum	23,319	2173	1266	10,002	154	7	8	3	52	36,984

Table A2. Land use/land cover area transfer matrix from the year 1992 to 2000 in the Turpan Basin.

Reclassified Class (km^2)	Bare Land	Cropland	Grassland	Permanent Snow and Ice	Settlement	Shrubland	Water	Wetland	Sum
Bare land	19,840	201	3163	35	38	14	11	56	23,359
Cropland	142	921	1029	0	78	10	0	0	2180
Forest	285	12	966	0	4	0	1	0	1269
Grassland	2400	49	7566	4	12	0	8	0	10,039
Permanent snow and ice	64	0	72	22	0	0	0	0	158
Settlement	0	1	0	0	6	0	0	0	7
Shrubland	7	0	1	0	0	0	0	0	8
Water	1	0	0	0	0	0	2	1	3
Wetland	2	0	0	0	0	0	6	44	52
Sum	22,741	1184	12,797	62	138	24	29	100	37,076

Table A3. Land use/land cover area transfer matrix from the year 2000 to 2010 in the Turpan Basin.

Reclassified Class (km^2)	Bare Land	Cropland	Grassland	Permanent Snow and Ice	Settlement	Shrubland	Water	Wetland	Sum
Bare land	22,497	116	122	1	17	2	2	0	22,757
Cropland	2	1162	11	0	9	0	0	0	1184
Grassland	387	26	12394	1	6	0	1	0	12,815
Permanent snow and ice	2	0	0	61	0	0	0	0	63
Settlement	1	15	1	0	122	0	0	0	138
Shrubland	1	4	0	0	0	19	0	0	24
Water	1	0	1	0	0	0	27	0	29
Wetland	0	0	0	0	0	0	0	100	100
Sum	22,890	1323	12,529	63	154	21	31	100	37,111

Table A4. Land use/land cover area transfer matrix from the year 2010 to 2020 in the Turpan Basin.

Reclassified Class (km^2)	Bare Land	Cropland	Forest	Grassland	Permanent Snow and Ice	Settlement	Shrubland	Water	Wetland	Sum
Bare land	22,362	57	0	304	32	128	3	2	0	22,890
Cropland	9	1229	0	27	0	56	0	1	0	1323
Grassland	357	166	27	11,906	11	56	0	2	2	12,529
Permanent snow and ice	3	0	0	0	60	0	0	0	0	63
Settlement	6	14	0	2	0	132	0	0	0	154
Shrubland	3	1	0	0	0	0	17	0	0	21
Water	24	0	0	2	0	1	0	4	0	31
Wetland	100	0	0	0	0	0	0	0	0	100
Sum	22,864	1467	27	12,243	104	374	20	9	3	37,111

Value	Label
0	No Data
10	Cropland, rainfed
11	Herbaceous cover
12	Tree or shrub cover
20	Cropland, irrigated or post-flooding
30	Mosaic cropland (>50%) / natural vegetation (tree, shrub, herbaceous cover) (<50%)
40	Mosaic natural vegetation (tree, shrub, herbaceous cover) (>50%) / cropland (<50%)
50	Tree cover, broadleaved, evergreen, closed to open (>15%)
60	Tree cover, broadleaved, deciduous, closed to open (>15%)
61	Tree cover, broadleaved, deciduous, closed (>40%)
62	Tree cover, broadleaved, deciduous, open (15-40%)
70	Tree cover, needleleaved, evergreen, closed to open (>15%)
71	Tree cover, needleleaved, evergreen, closed (>40%)
72	Tree cover, needleleaved, evergreen, open (15-40%)
80	Tree cover, needleleaved, deciduous, closed to open (>15%)
81	Tree cover, needleleaved, deciduous, closed (>40%)
82	Tree cover, needleleaved, deciduous, open (15-40%)
90	Tree cover, mixed leaf type (broadleaved and needleleaved)
100	Mosaic tree and shrub (>50%) / herbaceous cover (<50%)
110	Mosaic herbaceous cover (>50%) / tree and shrub (<50%)
120	Shrubland
121	Evergreen shrubland
122	Deciduous shrubland
130	Grassland
140	Lichens and mosses
150	Sparse vegetation (tree, shrub, herbaceous cover) (<15%)
152	Sparse shrub (<15%)
153	Sparse herbaceous cover (<15%)
160	Tree cover, flooded, fresh or brakish water
170	Tree cover, flooded, saline water
180	Shrub or herbaceous cover, flooded, fresh/saline/brakish water
190	Urban areas
200	Bare areas
201	Consolidated bare areas
202	Unconsolidated bare areas
210	Water bodies
220	Permanent snow and ice

Figure A1. The classification standard for CCI land cover [58]. As the CCI-LC maps are designed to be globally consistent, their legend is determined by the level of information that is available and that makes sense at the scale of the entire world. The "level 1" legend (also called "global" legend) counts 22 classes and each class is associated with a 10-value code (i.e., class codes of 10, 20, 30, etc.). The CCI-LC maps are also described by a more detailed legend, called "level 2" or "regional". This level 2 legend makes use of more accurate and regional information (where available). This regional legend has, therefore, more classes. The regional classes are associated with non-ten values (i.e., class codes such as 11, 12, etc.). They are not present all over the world since they were not properly discriminated at the global scale.

References

1. Ablimiti, N. Study on the Karez System and Its Influence on Ecological Environment in Turpan Area as an Example. Master's Thesis, Xinjiang University, Urumqi, China, 2015.
2. Wang Yujian, W.S. Comparative Study on Qanat in Kazan of Iran and Turpan of Xinjiang. *Agric. Archaeol.* **2021**, *1*, 134–140.
3. Al-Kindi, K.M.; Janizadeh, S. Machine Learning and Hyperparameters Algorithms for Identifying Groundwater Aflaj Potential Mapping in Semi-Arid Ecosystems Using LiDAR, Sentinel-2, GIS Data, and Analysis. *Remote Sens.* **2022**, *14*, 5425. [CrossRef]
4. Encyclopedia, B. Tentative List of World Cultural Heritage Sites of China. Website. 2022. Available online: https://baike.baidu.com/item/%E4%B8%AD%E5%9B%BD%E4%B8%96%E7%95%8C%E6%96%87%E5%8C%96%E9%81%97%E4%BA%A7%E9%A2%84%E5%A4%87%E5%90%8D%E5%8D%95/4181009 (accessed on 12 January 2023).
5. Mächtle, B.; Hecht, S.; Manke, N.; Kromer, B.; Lindauer, S.; Li, C.S.; Li, Y.; Wang, X.; Bubenzer, O. The Age and Origin of Karez Systems of Silk Road Oases around Turpan, Xinjiang, P.R. of China. In *Socio-Environmental Dynamics along the Historical Silk Road*; Springer: Cham, Switzerland, 2019; Book Section Chapter 17, pp. 359–378. [CrossRef]
6. Centre, U.W.H. The Persian Qanat. Website. 2016. Available online: https://whc.unesco.org/en/list/1506/ (accessed on 12 July 2022).
7. Remmington, G. Transforming tradition: The aflaj and changing role of traditional knowledge systems for collective water management. *J. Arid Environ.* **2018**, *151*, 134–140. [CrossRef]
8. Voudouris, K.; Christodoulakos, Y.; Steiakakis, E.; Angelakis, A. Hydrogeological Characteristics of Hellenic Aqueducts-Like Qanats. *Water* **2013**, *5*, 1326–1345. [CrossRef]
9. Radaei, M.; Salehi, E.; Faryadi, S.; Masnavi, M.R.; Zebardast, L. Ecological wisdom, a social–ecological approach to environmental planning with an emphasis on water resources: The case of Qanat Hydraulic Structure (QHS) in a desert city of Iran. *Environ. Dev. Sustain.* **2020**, *23*, 10490–10511. [CrossRef]
10. Moghadam, H.M.; Bagheri, R.; Karami, G.H.; Jafari, H. Groundwater Origin in Qanats, Chemo-Isotopic, and Hydrogeological Evidence. *Ground Water* **2020**, *58*, 771–776. [CrossRef]
11. Naghedifar, S.M.; Ziaei, A.N.; Naghedifar, S.A.; Ansari, H. A new model for simulation of collection and conveyance sections of Qanat. *J. Hydrol.* **2020**, *590*, 125218. [CrossRef]
12. Sedghi, M.M.; Zhan, H. Semi-analytical solutions of discharge variation of a qanat in an unconfined aquifer subjected to general areal recharge and nearby pumping well discharge. *J. Hydrol.* **2020**, *584*, 124691. [CrossRef]
13. Kazemi, A.; Esmaeilbeigi, M.; Sahebi, Z.; Ansari, A. Health risk assessment of total chromium in the qanat as historical drinking water supplying system. *Sci Total Environ.* **2022**, *807*, 150795. [CrossRef] [PubMed]
14. Pueppke, S. Ancient WEF: Water–Energy–Food Nexus in the Distant Past. *Water* **2021**, *13*, 925. [CrossRef]
15. Mirani Moghadam, H.; Karami, G.H.; Bagheri, R.; Barati, R. Death time estimation of water heritages in Gonabad Plain, Iran. *Environ. Earth Sci.* **2021**, *80*, 127. [CrossRef]
16. Velasco-Sánchez, Á.; Driessen, M.J.; Abudanah, F.; Nobels, P.R.; Comans, R.N.J.; Hoosbeek, M.R. Soil chemical changes in ancient irrigated fields of Udhruḥ, southern Jordan. *Geoarchaeology* **2021**, *37*, 374–384. [CrossRef]
17. Kowkabi, L. Revitalization of bio infrastructure network, an approach to urban regeneration: A case study of the qanats of Tehran. *Urban For. Urban Green.* **2021**, *59*, 127020. [CrossRef]
18. Delfani, S.; Esmaeelian, J.; Karami, M. Experimental investigation on the thermal performance of a qanat-source heat pump. *Geothermics* **2021**, *89*, 101933. [CrossRef]
19. Nasirian, A.; Maghrebi, M.F.; Mohtashami, A. Numerical and Experimental Assessment of Suspended Material Effects on Water Loss Reduction from Irrigation Channels. *Iran. J. Sci. Technol. Trans. Civ. Eng.* **2022**, *46*, 2483–2493. [CrossRef]
20. Barbaix, S.; De Maeyer, P.; Chen, X.; Bourgeois, J.; Kurban, A. An integrated approach to modelling the interaction of the natural landscape and the karez water system in Turpan (Xinjiang, P.R.C.). *Landsc. Res.* **2022**, *47*, 1052–1070. [CrossRef]
21. Manian, M.A.; Khoshbakht, K.; Mahmoudi, H.; Liaghati, H. Dynamic Conservation in Risk Society: A Case Study of COVID-19 Pandemic Risk in Kashan Qanat Irrigated Agriculture. *Front. Public Health* **2022**, *10*, 882943. [CrossRef] [PubMed]
22. Keramati, H.; Ghorbani, R.; Fakhri, Y.; Mousavi Khaneghah, A.; Conti, G.O.; Ferrante, M.; Ghaderpoori, M.; Taghavi, M.; Baninameh, Z.; Bay, A.; et al. Radon 222 in drinking water resources of Iran: A systematic review, meta-analysis and probabilistic risk assessment (Monte Carlo simulation). *Food Chem. Toxicol.* **2018**, *115*, 460–469. [CrossRef]
23. Ghosh, S.; Sharma, S.; Gadpayle, A.K.; Gupta, H.K.; Mahajan, R.K.; Sahoo, R.; Kumar, N. Review of Risk Assessment and Mitigation Measures of Coastal Aquifers Vulnerable to Saline Water Intrusion. *J. Trop. Med.* **2014**, *2014*, 142382. [CrossRef]
24. Sudip, B.; Loganathan, M.K.; Ghritartha, G.; Hadi, K. Saltwater Intrusion into Coastal Aquifers and Associated Risk Management: Critical Review and Research Directives. *J. Coast. Res.* **2022**, *38*, 654–672. [CrossRef]
25. Samani, S.; Vadiati, M.; Delkash, M.; Bonakdari, H. A hybrid wavelet–machine learning model for qanat water flow prediction. *Acta Geophys.* **2022**, 1–10. [CrossRef]
26. Karami, M.; Abdshahi, H. Energy and exergy analysis of the transient performance of a qanat-source heat pump using TRNSYS-MATLAB co-simulator. *Energy Environ.* **2022**, 0958305X211068152. [CrossRef]
27. Sedghi, M.M.; Zhan, H. On the discharge variation of a qanat in an alluvial fan aquifer. *J. Hydrol.* **2022**, *610*, 127922. [CrossRef]
28. Luo, L.; Wang, X.; Guo, H. Remote sensing archaeology: The next century. *Innovation* **2022**, *3*, 100335. [CrossRef]

29. Luo, L.; Wang, X.; Guo, H.; Lasaponara, R.; Zong, X.; Masini, N.; Wang, G.; Shi, P.; Khatteli, H.; Chen, F.; et al. Airborne and spaceborne remote sensing for archaeological and cultural heritage applications: A review of the century (1907–2017). *Remote Sens. Environ.* **2019**, *232*, 111280. [CrossRef]
30. Yang, S.; Luo, L.; Li, Q.; Chen, Y.; Wu, L.; Wang, X. Auto-identification of linear archaeological traces of the Great Wall in northwest China using improved DeepLabv3+ from very high-resolution aerial imagery. *Int. J. Appl. Earth Obs. Geoinf.* **2022**, *113*, 102995. [CrossRef]
31. Guo, H.; Liang, D.; Sun, Z.; Chen, F.; Wang, X.; Li, J.; Zhu, L.; Bian, J.; Wei, Y.; Huang, L.; et al. Measuring and evaluating SDG indicators with Big Earth Data. *Sci. Bull.* **2022**, *67*, 1792–1801. [CrossRef]
32. Guo, H.; Nativi, S.; Liang, D.; Craglia, M.; Wang, L.; Schade, S.; Corban, C.; He, G.; Pesaresi, M.; Li, J.; et al. Big Earth Data science: An information framework for a sustainable planet. *Int. J. Digit. Earth* **2020**, *13*, 743–767. [CrossRef]
33. Guo, H.; Liang, D.; Chen, F.; Shirazi, Z. Innovative approaches to the Sustainable Development Goals using Big Earth Data. *Big Earth Data* **2021**, *5*, 263–276. [CrossRef]
34. Guo, H.; Chen, F.; Sun, Z.; Liu, J.; Liang, D. Big Earth Data: A practice of sustainability science to achieve the Sustainable Development Goals. *Sci. Bull.* **2021**, *66*, 1050–1053. [CrossRef] [PubMed]
35. Gao, C.; Cheng, D.; Iqbal, J.; Yao, S. Spatiotemporal Change Analysis and Prediction of the Great Yellow River Region (GYRR) Land Cover and the Relationship Analysis with Mountain Hazards. *Land* **2023**, *12*, 340. [CrossRef]
36. Maghrebi, M.; Noori, R.; Sadegh, M.; Sarvarzadeh, F.; Akbarzadeh, A.E.; Karandish, F.; Barati, R.; Taherpour, H. Anthropogenic Decline of Ancient, Sustainable Water Systems: Qanats. *Ground Water* **2022**, *61*, 139–146. [CrossRef]
37. Halik, G. The Influence of Land Use Changes in Time and Space in Turpan Basin on Karez. Master's Thesis, Xinjiang Normal University, Urumqi, China, 2017.
38. Yang, J.; Huang, X. The 30 m annual land cover dataset and its dynamics in China from 1990 to 2019. *Earth Syst. Sci. Data* **2021**, *13*, 3907–3925. [CrossRef]
39. Laugier, E.J.; Casana, J. Integrating Satellite, UAV, and Ground-Based Remote Sensing in Archaeology: An Exploration of Pre-Modern Land Use in Northeastern Iraq. *Remote Sens.* **2021**, *13*, 5119. [CrossRef]
40. Valipour, M.; Ahmed, A.T.; Antoniou, G.P.; Sala, R.; Parise, M.; Salgot, M.; Sanaan Bensi, N.; Angelakis, A.N. Sustainability of Underground Hydro-Technologies: From Ancient to Modern Times and toward the Future. *Sustainability* **2020**, *12*, 8983. [CrossRef]
41. Sayadi, M.H.; Kharkan, J.; Binkowski, L.J.; Moshgani, M.; Blaszczyk, M.; Mansouri, B. Cadmium and chromium levels in water and edible herbs in a risk assessment study of rural residents living in Eastern Iran. *Environ. Sci. Pollut. Res. Int.* **2020**, *27*, 9901–9909. [CrossRef] [PubMed]
42. Zhang, Y.; Liu, X.; Yuan, S.; Zhang, T.; Song, J.; Chen, W. Probabilistic stability analysis of qanat tunnels in c-φ soil considering soil spatial variability. *Eur. J. Environ. Civ. Eng.* **2022**, 1–21. [CrossRef]
43. Ebrahimi, A.; Mehraban, Y.; Omidvarborna, H.; Vakilinejad, A.; Al-Sayigh, A.R.S. Kariz (Ancient Aqueduct) system: A review on geoengineering and environmental studies. *Environ. Earth Sci.* **2021**, *80*, 236. [CrossRef]
44. Xinjiang Second Surveying and Mapping Institute. *Distribution Map of Karez in Xinjiang Uyghur Autonomous Region*; Xinjiang Second Surveying and Mapping Institute: Urumqi, China, 2004.
45. Xinjiang Uyghur Autonomous Region Cultural Relics Bureau. *Integration of the Third National Cultural Relics Census Results in Xinjiang Uyghur Autonomous Region: Karez in Xinjiang*; Science Press: Beijing, China, 2011; p. 1639.
46. Institute of Tibetan Plateau Research of the Chinese Academy of Sciences (ITPCAS). *Landuse Dataset in China (1980–2015)*; National Tibetan Plateau/Third Pole Environment Data Center: Beijing, China, 2020.
47. Xu, X. *Global ESA CCI Land Cover Classification Map (1992–2015)*; National Tibetan Plateau/Third Pole Environment Data Center: Beijing, China, 2018.
48. Sun, W.; Ding, X.; Su, J.; Mu, X.; Zhang, Y.; Gao, P.; Zhao, G. Land use and cover changes on the Loess Plateau: A comparison of six global or national land use and cover datasets. *Land Use Policy* **2022**, *119*, 106165. [CrossRef]
49. Li, W.; MacBean, N.; Ciais, P.; Defourny, P.; Lamarche, C.; Bontemps, S.; Houghton, R.A.; Peng, S. Gross and net land cover changes in the main plant functional types derived from the annual ESA CCI land cover maps (1992–2015). *Earth Syst. Sci. Data* **2018**, *10*, 219–234. [CrossRef]
50. Tiandraza, F.; Qu, S.; Hu, S.; Mkono, C.N.; Tikhomirova, A.; Randrialahamady, S.N. Response of Ecosystem Services to Land Use Change in Madagascar Island, Africa: A Multi-Scale Perspective. *Int. J. Environ. Res. Public Health* **2023**, *20*, 3060. [CrossRef] [PubMed]
51. Tew, Y.L.; Tan, M.L.; Kwok, P.C.; Samat, N.; Mahamud, M.A. Analysis of the Relationship between Climate Change and Land Use Change using the ESA CCI Land Cover Maps in Sungai Kelantan Basin, Malaysia. *Sains Malays.* **2022**, *51*, 437–449. [CrossRef]
52. Chen, J.; Chen, J.; Liao, A.; Cao, X.; Chen, L.; Chen, X.; He, C.; Han, G.; Peng, S.; Lu, M.; et al. Global land cover mapping at 30m resolution: A POK-based operational approach. *ISPRS J. Photogramm. Remote Sens.* **2015**, *103*, 7–27. [CrossRef]
53. Abudu, S.; Sheng, Z.; King, J.P.; Ahn, S.R. A Karez System's Dilemma: A Cultural Heritage on a Shelf or Still a Viable Technique for Water Resiliency in Arid Regions. In *Socio-Environmental Dynamics along the Historical Silk Road*; Yang, L.E., Bork, H.R., Fang, X., Mischke, S., Eds.; Springer International Publishing: Cham, Switzerland, 2019; pp. 507–525. [CrossRef]
54. Mamati, R. Study on The Relationship Between the Karez and Turpan Oasis Ecological Environment. Master's Thesis, Xinjiang University, Urumqi, China, 2014.

55. Li, K.; Li, Z.; Gao, W.; Wang, L. Recent glacial retreat and its effect on water resources in eastern Xinjiang. *Chin. Sci. Bull.* **2011**, *56*, 3596–3604. [CrossRef]
56. Li, Q.; Guo, H.; Luo, L.; Wang, X. Automatic Mapping of Karez in Turpan Basin Based on Google Earth Images and the YOLOv5 Model. *Remote Sens.* **2022**, *14*, 3318. [CrossRef]
57. Ma, L. Population. In *Xinjiang Yearbook*; China Academic Journal Electronic Publishing House: Beijing, China, 1985; p. 80.
58. ESA. Land Cover CCI Product User Guide Version 2. Technical Reports, 2017. Available online: maps.elie.ucl.ac.be/CCI/viewer/download/ESACCI-LC-Ph2-PUGv2_2.0.pdf (accessed on 14 November 2022).

Disclaimer/Publisher's Note: The statements, opinions and data contained in all publications are solely those of the individual author(s) and contributor(s) and not of MDPI and/or the editor(s). MDPI and/or the editor(s) disclaim responsibility for any injury to people or property resulting from any ideas, methods, instructions or products referred to in the content.